Structural study of monoclinic Li_2FeSiO_4 by X-ray diffraction and Mössbauer spectroscopy

Dragana Jugović[a], Miloš Milović[a], Valentin N. Ivanovski[b], Max Avdeev[c], Robert Dominko[d], Bojan Jokić[f], Dragan Uskoković[a]

[a]Institute of Technical Sciences of SASA, Knez Mihailova 35/IV, 11 000 Belgrade, Serbia

[b]Vinča Institute of Nuclear Sciences, University of Belgrade, P.O. Box 522, 11 001 Belgrade, Serbia

[c]Bragg Institute, Australian Nuclear Science and Technology Organisation, Locked Bag 2001, Kirrawee DC, NSW 2232, Australia

[d]National Institute of Chemistry, Hajdrihova 19, SI-1000 Ljubljana, Slovenia,

[f]Faculty of Technology and Metallurgy, University of Belgrade, Karnegijeva 4, 11 000 Belgrade, Serbia

Abstract

A composite powder Li_2FeSiO_4/C is synthesized through a solid state reaction at 750 °C. The Rietveld crystal structure refinement is done in the monoclinic $P2_1/n$ space group. It is found that the crystal structure is prone to “antisite” defect where small part of iron ion occupies exclusively Li(2) crystallographic position, of two different lithium tetrahedral

positions (Li(1) and Li(2)). This finding is also confirmed by Mössbauer spectroscopy study: the sextet evidenced in the Mössbauer spectrum is assigned to the iron ions positioned at the Li(2) sites. A bond-valence energy landscape calculation is used to predict the conduction pathways of lithium ions. The calculations suggest that Li conductivity is two-dimensional in the (101) plane. Upon galvanostatic cyclings the structure starts to rearrange to inverse β_{II} polymorph.

Keywords: Lithium iron silicate (Li_2FeSiO_4); Cathode material; Rietveld X-ray refinement; Mössbauer spectroscopy; Bond-valence energy landscape

Corresponding author: Dragana Jugović

Institute of Technical Sciences of SASA

Knez Mihailova 35/IV, 11 000 Belgrade, Serbia,

Phone: +381641177549,

Fax: +381112185263,

e-mail: dragana.jugovic@itn.sanu.ac.rs; djugovic@vinca.rs

1. Introduction

The increasing need for high density energy storage devices is a driving force for pursuit and development of new cathode materials for Li-ion batteries. Ever since Li_2FeSiO_4 was first introduced by Nytén et al. [1], lithium transition-metal orthosilicates with general formula Li_2MSiO_4 (M = Fe, Mn, etc.) have attracted a lot of interest due to their potentially high theoretical capacities arising from the possibility for the extraction

of two Li-ions per formula unit [2]. In addition, their intrinsic thermal and structural stability, as a result of strong Si-O bonds, together with low cost of raw materials and environmental friendliness further enhance their potential to become cathode materials of choice for large-scale battery applications.

There are several polymorphs of Li_2FeSiO_4 structure reported so far with different symmetries: *Pmnb*, $P2_1/n$, $Pmn2_1$ [3, 4]. All the cations, within these polymorph structures, are positioned in the tetrahedral sites in a slightly distorted hcp oxygen array, but with different interconnectivity of cation tetrahedra and their respective orientations along a given crystallographic direction [3, 5]. This is dissimilar to general electrochemically active transition metal compounds in which transition metal ions occupy octahedral sites. The common feature for Li_2FeSiO_4 polymorphs is that during electrochemical cycling the host structure transforms to inverse β_{II} structure [4, 6] as a more stable polymorph [7].

The structure of Li_2FeSiO_4 under investigation belongs to the monoclinic space group $P2_1/n$ (#14) and consists of a slightly distorted hexagonal close-packed (hcp) oxygen framework. The lithium, silicon, and iron atoms occupy 1/4, 1/8, and 1/8 of tetrahedral sites, respectively.. The structure can be considered as a layered one: Si and Fe atoms are forming (101) layers of corner-shared SiO_4 – FeO_4 tetrahedra (Fig. 1.). The FeO_4 tetrahedra have no common corners. The LiO_4 tetrahedra are positioned between two adjacent Si-Fe layers. There are two different lithium tetrahedral positions (here denoted as Li(1) and Li(2)): the $Li(1)O_4$ tetrahedra are arranged in edge sharing pairs with FeO_4 tetrahedra, while the $Li(2)O_4$ tetrahedra form edge sharing pairs with themselves. The $Li(1)O_4$ tetrahedra are corner-share interconnected.

In the present paper, Li_2FeSiO_4/C composite was synthesized by means of the solid-state reaction. Special attention has been paid to the refinement of the crystal structure, which indicates that the structure is prone to an antisite defect; that is the replacement of lithium and iron ions. The crystal structure refinement results were confirmed by Mössbauer spectroscopy. Additionally, the refined data were used for the mapping of Li^+ diffusion paths by the application of the bond valence model and a brief overview of transport properties is given at the end of the paper.

.

2. Experimental

Li_2FeSiO_4 was synthesized by a solid-state reaction of $Fe(NO_3)_3$*$9H_2O$, Li_2CO_3, SiO_2, and glucose. The starting compounds were mixed in the molar ratio of Li:Fe:Si = 2:1:1, dispersed in water, thoroughly ground after drying, and then calcined for 2 hours at 750 °C in a slightly reducingatmosphere (Ar + 5% H_2). Glucose was added (4 wt%) as a carbon source that on pyrolytic decomposition forms carbon impeding particle growth and maintains reducing atmosphere. The amount of the *in situ* formed carbon was determined thermogravimetrically and estimated at 1.3 wt%. Interestingly, when the calcinations temperature of 700 °C was used, Li_2FeSiO_4 did not form and instead the mixture of Li_2SiO_3 and Fe_3O_4 was obtained. However, an additional calcination of the mixture for one hour at 750 °C in the same atmosphere produced Li_2FeSiO_4. Therefore the temperature of 750 °C was chosen as the minimal required temperature for obtaining Li_2FeSiO_4 phase from the chosen starting materials.

The X-ray powder diffraction measurements were performed on a Philips 1050 X-ray powder diffractometer using Ni-filtered Cu K_α radiation and Bragg–Brentano focusing geometry. The patterns were taken in the 10 – 120° 2θ range with the step of 0.02° and exposure time of 15 s per step.

The thermal analysis of the sample was performed on a SDT 2960 simultaneous DSC–TGA TA Instruments in order to determine the carbon content.

The morphology of the synthesized powder was analyzed by scanning electron microscopy (TESCAN, MIRA3 XMU) at 20 kV.

The ^{57}Fe Mössbauer measurement was carried out in transmission mode by the Weissel velocity drive unit in a constant acceleration mode using a ^{57}Co (Rh) radioactive source at the room temperature. Velocity calibration of the spectrum was done by laser. The spectrum of natural iron foil was used to calibrate values of isomer shift of the powdered sample. The spectrum was analyzed with the WinNormos-Dist/Xls program which combined distribution of Mössbauer lines and subspectra, based on the histogram method and the least squares method, respectively [8].

Electrochemical measurements were carried out in a closed, argon filled two-electrode cell at room temperature, with metallic lithium as a counter electrode. 1M solution of $LiClO_4$ (p.a., Chemmetall GmbH) in PC (p.a., Honeywell) was used as an electrolyte. Working electrodes were made from the synthesized material, carbon black, and polyvinylidene fluoride (PVdF, Aldrich) mixed in 70:20:10 weight percent ratio and deposited on platinum foils from slurry prepared in N-methyl-2-pyrrolidone. Galvanostatic charge/discharge tests were performed between 4.0 and 1.5 V at C/20 and C/10 current rates.

3. Results and discussion

The morphology of the powder, as revealed by scanning electron microscopy, is shown in Fig. 2. The particles are irregular in shape, consisting of closely packed and sintered platelet-like structures, with an average particle size of 250 nm. Owing to the in situ formation of carbon, which impeded the particle growth, the particles are smaller in size than those typically found in powders prepared by solid-state reaction [9].

The crystal structure of the synthesized powder was confirmed by X-ray powder diffraction. The diffraction pattern revealed the Li_2FeSiO_4 phase of a monoclinic structure, with traces of Li_2SiO_3 as an impurity phase (Fig. 3). The structure of Li_2FeSiO_4 powder has been refined in the space group $P2_1/n$ (14. S.G.) in a structure type where Li^+, Fe^{2+}, and Si^{4+}, and O^{2-} ions occupy two, one, one and four different general 4*e* crystallographic positions [x,y,z], respectively. The crystal structure refinement was based on the Rietveld full profile method [10] using the Koalariet computing program based on the Fundamental Parameters convolution approach to generate line profiles [11]. The observed and calculated X-ray diffraction profiles of the sample are given in Fig. 3, while the main results of the final Rietveld refinement are presented in Tables 1 and 2. Lattice parameters are consistent with the literature data [3, 12]. Comparison of the average particle size determined by scanning electron microscopy with the mean crystallite size of 100 nm, determined from the X-ray diffraction data, implies polycrystalline nature of the powder particles. The Rietveld refinement also showed additional electron density on the lithium sites (negative Debye-Waller factor) indicating

a so-called "anti-site" defect in which a Li ion (on the Li(1) and/or Li(2) sites) and an Fe ion are interchanged. This antisite defect is found to be the most favourable defect of Li_2MSiO_4 structures [4, 13]. For that reason, during the refinements it was allowed for the Fe ions to also occupy both Li sites beside the Fe site. This approach resulted in the decrease of R values and the best refinement was achieved for the arrangement where ~5 at.% of the Fe ions occupy Li(2) crystallographic position, but not the Li(1) site. A possible explanation of such Fe accumulation only in one Li position can be found by examining the geometry of Li_2FeSiO_4 structure. The refined fractional atomic coordinates (Table 2) were used for the calculation of all relevant bond distances (Table 3) that enabled us to determine coordination polyhedra (Fig. 4), bond valence sums (Table 2), and polyhedra distortion (Table 4). Bond valence sums, V_i, were calculated as a sum of bond valences, s_{ij}, using the equation: $s=\exp[(ro-r)/B]$, where ro and B are empirical parameters [14] and r is the bond length from the refined structural model. The global instability index of 0.24 vu implies presence of a substantial strain in the structure.

The crystal structure of Li_2FeSiO_4 has four different types of oxygen atoms, which form tetrahedra around Fe, Li and Si atoms. Each FeO_4 tetrahedron shares three vertices with four $Li(2)O_4$ tetrahedra and an edge and two vertices with three $Li(1)O_4$ tetrahedra. If an iron ion occupies a Li(1) position, then two adjacent edge-shared Fe tetrahedra would occur, while only the corner-shared Fe tetrahedra would occur if the replacement takes place at a Li(2) site. Two different scenarios would result in Fe-Fe interatomic distances of 2.64 and 2.91 Å, respectively. According to the Pauling's rules, cations prefer to maintain maximum separation from the other cations that are their second nearest neighbors. Therefore, it may be expected that a small amount of Fe would

exchange places with lithium ion preferably at Li(2) sites to minimize Fe-Fe second nearest-neighbor cation interactions.

The Mössbauer spectrum consists of four subspectra: one doublet, one sextet and two single line distributions (Fig.5). The Mössbauer parameters are given in Table 5. The doublet has its origin from Li_2FeSiO_4 [15]. There is only one inequivalent position of Fe ion in the $P2_1/n$ polymorph. The isomer shift is 0.959(1) mms^{-1}, which is in the upper limit of the characteristic values for tetrahedral environment of Fe^{2+} cations. This implies that a negative charge is removed from the iron nucleus causing an increase of the isomer shift value. The distortion of the FeO_4 tetrahedron (Table 4 and Fig. 4) contributes to a large value of quadrupole splitting of 2.391(1) mms^{-1}, already reported in the literature [16]. This doublet, with 81.7(3) % of total fitted area, is the main contribution to the spectrum, and assuming that the recoilless factors are the same for all Fe sites, 81.7 % is the volume fraction of this phase. Likewise, the line width is narrow, 0.271(1) mms^{-1}, indicating that the doublet originates from the well positioned Fe ions, and thus excluding the presence of other Li_2FeSiO_4 polymorphs in the sample [15].

The sextet evidenced in the Mössbauer spectrum could be assigned to the iron ions positioned at the lithium sites (Li(1) or Li(2)). As discussed above, there are two inequivalent positions of lithium ions in the $P2_1/n$ polymorph, with different polyhedra distortion: Li(1) polyhedron distortion being almost four times higher than that of Li(2) (Table 4 and Fig. 4). Supposing that Fe ion is positioned at the more distorted Li(1) site, due to a greater distortion of that site in a comparison with that of the Li(2) site, it would be exposed to stronger electric field gradient (EFG), which would give rise to quadrupole shift. Considering the obtained small value for the quadrupole shift (2ε) of the sextet of

0.2(1) mms^{-1}, to be the measurement of the interaction between the nuclear quadrupole moment of cation probe and EFG, we are concluding that Fe ion substitutes Li ion at the Li(2) site. Quite large line widths of the sextet of 0.9(2) mms^{-1} reflect the distortion of that site. The sextet isomer shift of 0.82(6) mms^{-1} confirms the tetrahedral coordination of Fe^{2+}, although that value is approaching the values for the planar environment [17]. Additional confirmation that part of iron ions are exclusively positioned at the Li(2) site is found from the bond valence calculations. If the Fe ion is placed on the Li(2) or Li(1) position without the disruption of polyhedra geometries, then the Fe valences would be 2.0 and 2.4 v.u., respectively, as predicted by the bond valence model. For the iron ion positioned at Li(1) site the mean oxidation state would be higher than +2, which would be reflected on the value of sextet isomer shift. The magnitude of the hyperfine magnetic interaction which the iron nuclei on Li(2) sites are exposed to is 30.6(4) T, and it can be associated with ferromagnetic superexchange interactions. The angles of superexchange interactions Fe^{2+} - O^{2-} - Fe^{2+} of around 104.6˚, 110.1˚, 89.7˚, and 103.4˚, deviate from ideal ferromagnetic superexchange geometry [18]. Contribution to the whole fitted area of the sextet is 6.3 %, while the rescaled value to the amount of Li_2FeSiO_4 compound is 7.1 %, which is in quite good agreement with the results of the Rietveld refinement (Table 1).

The third and fourth subspectra are single Lorentzians. which represent the Mössbauer signal from stoichiometric and nonstoichiometric magnetite nanopowder. The magnetite is a spinel ferrite arranged as $[Fe^{3+}]_{tetrahedral}[Fe^{2+}Fe^{3+}]_{octahedral}O_4$. The Mössbauer parameters for the bulk magnetite are: δ=0.26 mms^{-1}, Δ=-0.02 mms^{-1}, and B_{hf}=49 T for the tetrahedral site, and δ=0.67 mms^{-1}, Δ=0 mms^{-1}, and B_{hf}=46 T for the octahedral site

[19]. With the decrease of particle volume, superparamagnetism may occur, when the measurement of hyperfine field is impossible. The first singlet is represented by the unimodal distribution, with the average isomer shift of 0.645 mms^{-1}, and the standard deviation of 0.152 mms^{-1}. This isomer shift is a result of the fast electron hopping between Fe^{2+} and Fe^{3+} on the octahedral sites. Its fraction is 10.3(7) % of the total fitted area. The second distribution is bimodal distribution presenting 1.7(1) % of the total fitted area. This distribution is a signal from the octahedral sites where existing vacancies break down electron hopping at the unpaired Fe^{2+} and Fe^{3+} cations [20]. The distribution is related to the structural distortion of the environment of the absorbing ion probably associated with the amorphous or nanoparticulate nature of this phase, which is not detectable by X-ray diffraction due to its low crystallinity.

Empirical bond length–bond valence relations provide insight into the link between the structure and ion transport. Knowing the structure opens up the possibility to utilize the bond-valence approach to find the diffusion pathways of lithium ions in the crystal lattice. It is based on an assumption that any point in the unit cell having a value of 1.0 vu represents a possible location for Li^{+} [21]. The 3DBVSMAPPER program was used to calculate the spatial distributions of bond-valence sum values on a three-dimensional grid, and to identify infinitely connected isosurfaces in these spatial distributions for a given bond-valence energy threshold and to extract their volume and surface area characteristics [22]. The calculations suggest that Li conductivity is two-dimensional in the (101) layer (Fig. 6) with overall diffusion via curved trajectories in the *b* direction and along the diagonal between the *a*- and *c*-axes. This finding is in a good agreement with the calculated activation energies for Li-ion migration in isostructural

Li_2MnSiO_4 [13], which showed a very high activation barrier perpendicular to the (101) layers. Anti-site defect (an Fe ion positioned at the Li site) within such conductivity network will impede Li-ion migration. At the same time, presence of Li at the Fe sites may be expected to provide Li transfer between the conducting layers and thus improve overall ionic conductivity of the material by making it three-dimensional, although the concentration of such defects should be high for good percolation.

An *ex situ* diffraction experiment was performed on the material taken from the cycled electrode in order to verify the crystal structure sustainability (inset of Fig. 7). It is evident that the charging process leads to structural rearrangement though it was not possible to refine the new structure due to a poor signal to noise ratio of the XRD pattern. However, some conclusions can be derived by the comparison with the literature data and it appears that the phase transformation towards inverse β_{II} polymorph starts to occur [4]. Discharge curve profile (Fig. 7) does not reflect a two-phase intercalation reaction (no obvious voltage plateau) due to the low conductivity at room temperature and it is typically observed for the room-temperature cycling of silicates [23].

4. Conclusions

Monoclinic Li_2FeSiO_4 polymorph that crystallizes in $P2_1/n$ space group was synthesized by means of the solid-state reaction at 750 °C. A combined X-ray diffraction and Mössbauer spectroscopy study revealed that the structure of the specimen is prone to an antisite defect, the one in which the Fe ion and the Li ion exchange places. Furthermore, it was found that an iron ion replaces a lithium ion exclusively at the Li(2)

position. This phenomenon was ascribed to the electrostatic repulsions between cations. The bond-valence sum map method suggests that Li conductivity is two-dimensional in the (101) layer. After several galvanostatic cyclings the structural rearrangement to inverse β_{II} polymorph was noticed.

Acknowledgements

The authors would like to express their gratitude to Dr. Miodrag Mitrić for great help and valuable suggestions. The Ministry of Education, Science and Technological Development of the Republic of Serbia provided financial support for this study under grants nos. III 45004, 171001 and bilateral project between the Republic of Slovenia and the Republic of Serbia no. 651-03-1251/2012-09/05.

References

[1] A. Nyten, A. Abouimrane, M. Armand, T. Gustafsson, J.O. Thomas, Electrochem. Commun. 7 (2005) 156-160.

[2] A. Kokalj, R. Dominko, G. Mali, A. Meden, M. Gaberscek, J. Jamnik, Chem. Mater. 19 (2007) 3633-3640.

[3] C. Sirisopanaporn, C. Masquelier, P. G. Bruce, A. R. Armstrong, R. Dominko, J. Am. Chem. Soc. 133 (2011) 1263-1265.

[4] A. R. Armstrong, N. Kuganathan, M. S. Islam, P. G. Bruce, J. Am. Chem. Soc. 133 (2011) 13031-13035.

[5] A. Liivat, Solid State Ionics 228 (2012) 19-24.

[6] H. Zhou, M. Einarsrud, F. Vullum-Bruer, J. Power Sources 238 (2013) 478-484.

[7] D. Seo, H. Kim, I. Park, J. Hong, K. Kang, Phys. Rev. B 84 (2011) 220106(R).

[8] R. A. Brand, WinNormos Mössbauer fitting program, Universität Duisburg, Duisburg, 2008.

[9] C. Sirisopanaporn, A. Boulineau, D. Hanzel, R. Dominko, B. Budic, A. R. Armstrong, P. G. Bruce, C. Masquelier, Inorg. Chem. 49 (2010) 7446-7451.

[10] H. M. Rietveld, J. Appl. Cryst. 2 (1969) 65-71.

[11] R. W. Cheary, A. Coelho, J. Appl. Cryst. 25 (1992) 109-121.

[12] M. Dahbi, S. Urbonaite, T. Gustafsson, J. Power Sources 205 (2012) 456-462.

[13] C. A. J. Fisher, N. Kuganathan, M. S. Islam, J. Mater. Chem. A 1 (2013) 4207-4214.

[14] I. D. Brown, D. Altermatt, Acta Cryst. B 41 (1985) 244-247.

[15] G. Mali, C. Sirisopanaporn, C. Masquelier, D. Hanzel, R. Dominko, Chem. Mater. 23 (2011) 2735-2744.

[16] I. K. Lee, S. J. Kim, T. Kouh, C. S. Kim, J. Appl. Phys. 113 (2013) 17E306.

[17] N. N. Greenwood, T. C. Gibb, Mössbauer Spectroscopy, Chapman and Hall Ltd, London, 1971.

[18] E. Pavarini, E. Koch, F. Anders, M. Jarrell, Correlated Electrons: From models to Materials Modeling and Simulation Vol. 2, Forschungszentrum Jülich, 2012, pp. 7.13-7.17.

[19] R. M. Cornell, U. Schwertmann, The iron oxides: Structure, properties, reactions, occurrence, and use, VCH, Weinheim, 1996, pp. 120-123.

[20] J. M. Daniels, A. Rosencwaig, J. Phys. Chem. Solids 30 (1969) 1561-1571.

[21] I. D. Brown, Chem. Rev. 109 (2009) 6858-6919.

[22] M. Sale, M. Avdeev, J. Appl. Cryst. 45 (2012) 1054-1056.

[23] Z. Zheng, Y. Wang, A. Zhang, T. Zhang, F. Cheng, Z. Tao, J. Chen, J. Power Sources 198 (2012) 229-235.

Table1. The final results of the Rietveld refinement.

Lattice parameters (Å)	a = 8.2329(14) Å b = 5.0196(2) Å c = 8.2347(14) Å β = 99.107(3)°
Cell volume ($Å^3$)	336.02(8)
Mean crystallite size (nm)	100(6)
Li-site (Li2) occ. by Fe	0.05(1)
R_{wp} factor (%)	1.293

Table 2. Refined fractional coordinates, overall isotropic temperature factor and the bond valence sum.

fractional coordinates	Wyckoff site	x	y	z	B_{ov} ($Å^2$)	Valence sum (v.u.)
Li(1)	4e	0.6499(4)	0.8974(10)	0.7071(6)		1.17(5)
Li(2)	4e	0.5876(5)	0.2359(5)	0.0699(7)		0.96(6)
Fe	4e	0.2931(7)	0.8013(7)	0.5412(7)		1.72(6)
Si	4e	0.0416(1)	0.8124(2)	0.7958(1)		4.26(8)
O(1)	4e	0.8658(11)	0.7174(10)	0.8174(2)	0.43(7)	2.4(1)
O(2)	4e	0.4139(2)	0.2077(3)	0.8828(2)		1.9(1)
O(3)	4e	0.6878(2)	0.7698(2)	0.4352(5)		1.9(2)
O(4)	4e	0.9704(2)	0.8674(2)	0.2142(2)		1.91(6)

Table 3. Bond lengths of MO_4 tetrahedra.

M-O bond	(Å)
Li(1)-O(1)	1.622(7)
Li(1)-O(1)	2.071(9)
Li(1)-O(4)	1.995(4)
Li(1)-O(3)	2.396(6)
(Li1-O)av	2.021(7)
Li(2)-O(4)	2.023(5)
Li(2)-O(2)	1.934(5)
Li(2)-O(3)	1.864(5)
Li(2)-O(2)	2.261(3)
(Li2-O)av	2.021(5)
Fe-O(2)	1.963(6)
Fe-O(4)	2.054(6)
Fe-O(1)	2.028(7)
Fe-O(3)	2.165(5)
(Fe-O)av	2.052(6)
Si-O(1)	1.561(9)
Si-O(3)	1.581(3)
Si-O(4)	1.612(1)
Si-O(2)	1.656(2)
(Si-O)av	1.602(4)

Table 4. The distortion parameter of MO_4 tetrahedra defined as $D = (1/4) \sum_n [(d_n - \langle d \rangle) / \langle d \rangle]^2$ with an average MO distance $\langle d \rangle$.

MO_4 tetrahedron	D
Li (1)	19×10^{-3}
Li (2)	5.0×10^{-3}
Fe	1.3×10^{-3}
Si	0.5×10^{-3}

Table 5. Mössbauer parameters: A-relative area fraction of a component, Γ-line width (FWHM), δ- isomer shift with respect to the α-Fe, Δ-quadrupole splitting (2ε- quadrupole shift) and B- hyperfine induction.

Compound	Site	Mössbauer parameters				
		A	Γ	δ	Δ / 2ε	B
		[%]	[mms^{-1}]	[mms^{-1}]	[mms^{-1}]	[T]
Li_2FeSiO_4	Fe	81.7(3)	0.271(1)	0.959(1)	2.391(1)	
	Fe→Li(2)	6.3(1.3)	0.9(2)	0.82(6)	-0.2(1)	30.6(4)
Distributions:				<δ>	SD	
Fe_3O_4		10.3(7)		0.663	0.152	
		1.7(1)		1.185	0.093	

Figure captions

Fig. 1. The structure of Li_2FeSiO_4 projected along b axis.

Fig. 2. FESEM micrograph of the synthesized powder.

Fig. 3. The observed (•), calculated (-), and the difference between the observed and calculated (bottom) X-ray diffraction data taken at room temperature. Vertical markers below the diffraction patterns indicate positions of possible Bragg reflections for monoclinic Li_2FeSiO_4. The asterisk shows the position of the strongest Li_2SiO_3 reflection.

Fig. 4. LiO_4 coordination tetrahedra.

Fig. 5. The Mössbauer spectrum of Li_2FeSiO_4/C at the room temperature. The values of relative absorption and residual`s width are shown. The fitted lines of subspectra are plotted above the main spectrum with fitted line. Inset shows two single line distributions.

Fig. 6. a) Bond valence model of Li^+ migration paths in monoclinic Li_2FeSiO_4 displayed as isosurface of constant E(Li); b) Projection of Li^+ migration paths in the (101) layer.

Fig. 7. Discharge curves of the synthesized powders at C/20 and C/10 rates. Inset: The X-ray diffractogram taken from the cycled material, after the charging process.

Figure 1

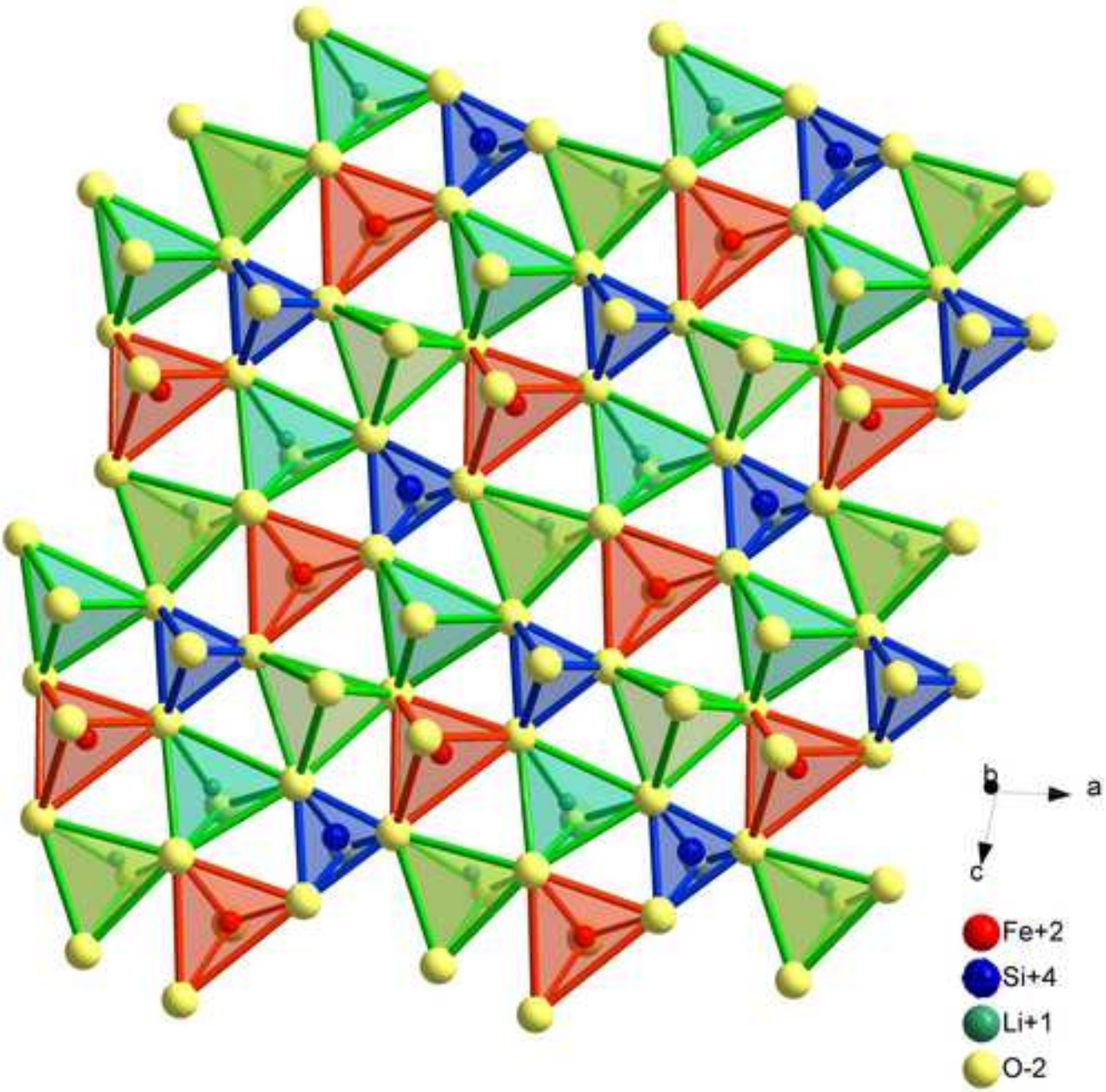

Figure 2

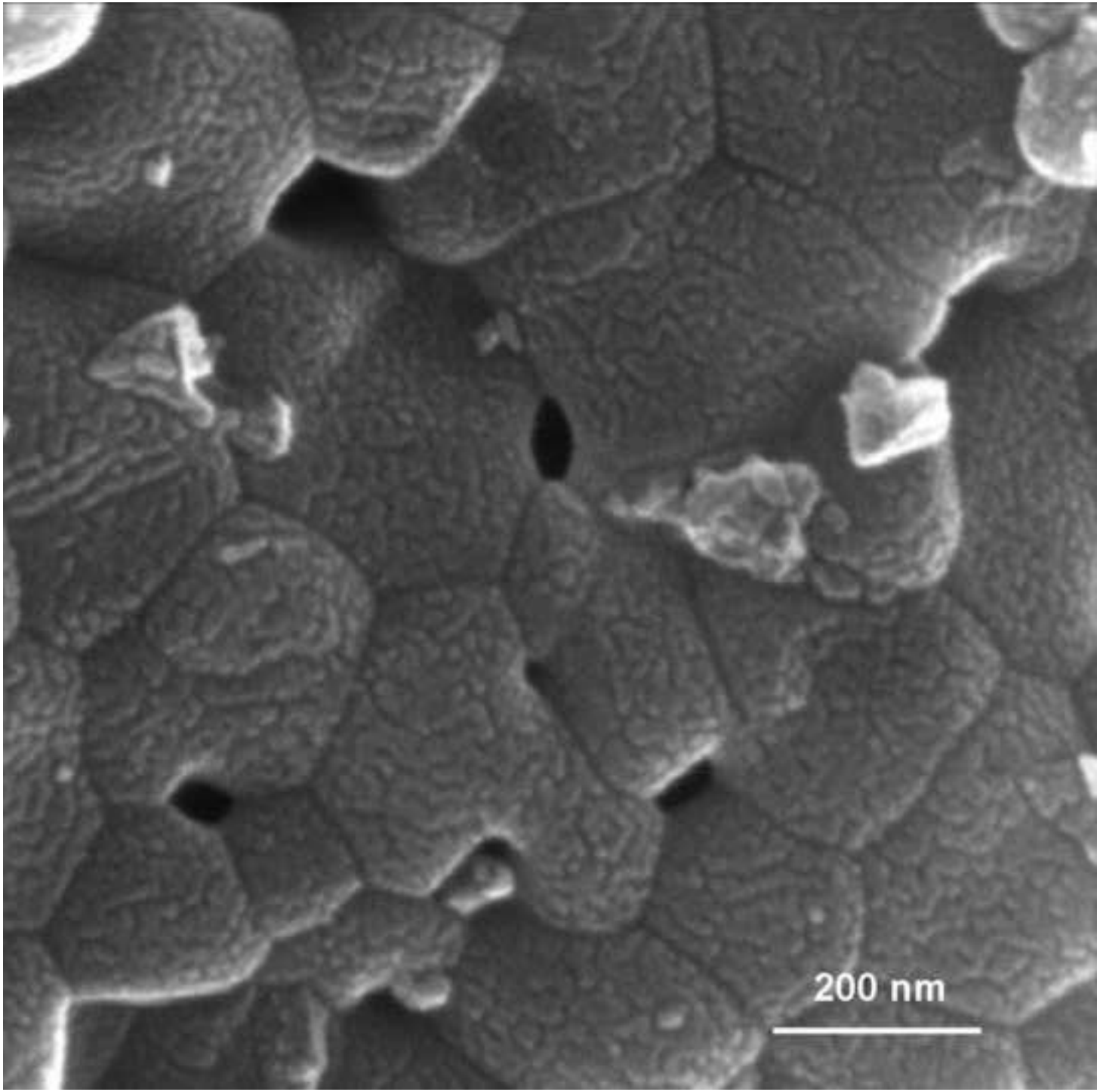

Figure 3

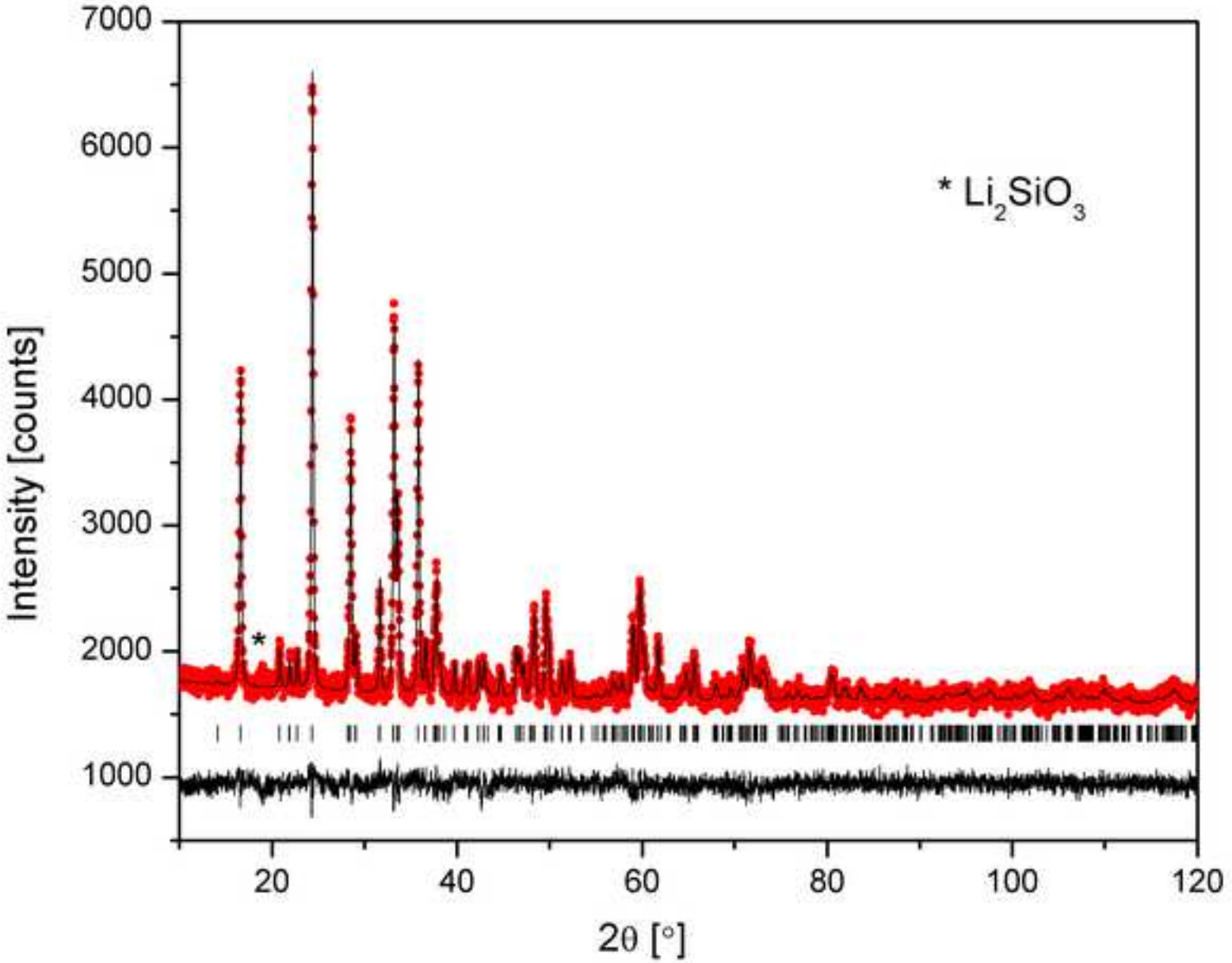
7000
6000
5000
4000
3000
2000
1000
Intensity [counts]
* Li2SiO3
*
20
40
60
80
100
120
2θ [°]

Figure 4

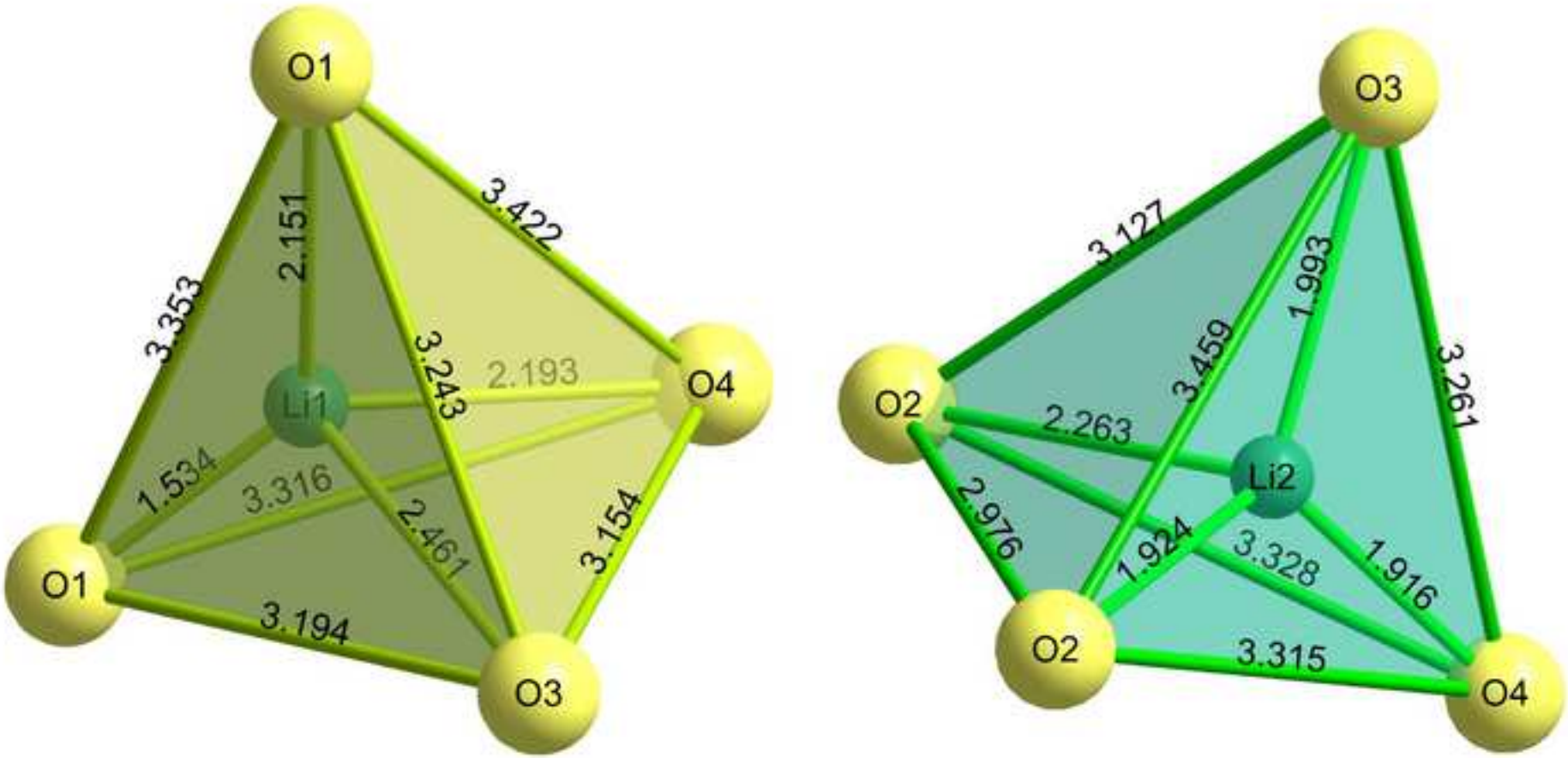
O1
2.151
3.422
3.353
3.243
2.193
O4
Li1
1.534
3.316
2.461
3.154
O1
3.194
O3
O3
3.127
1.993
3.459
3.261
O2
2.263
Li2
2.976
1.924
3.328
1.916
O2
3.315
O4

Figure 5

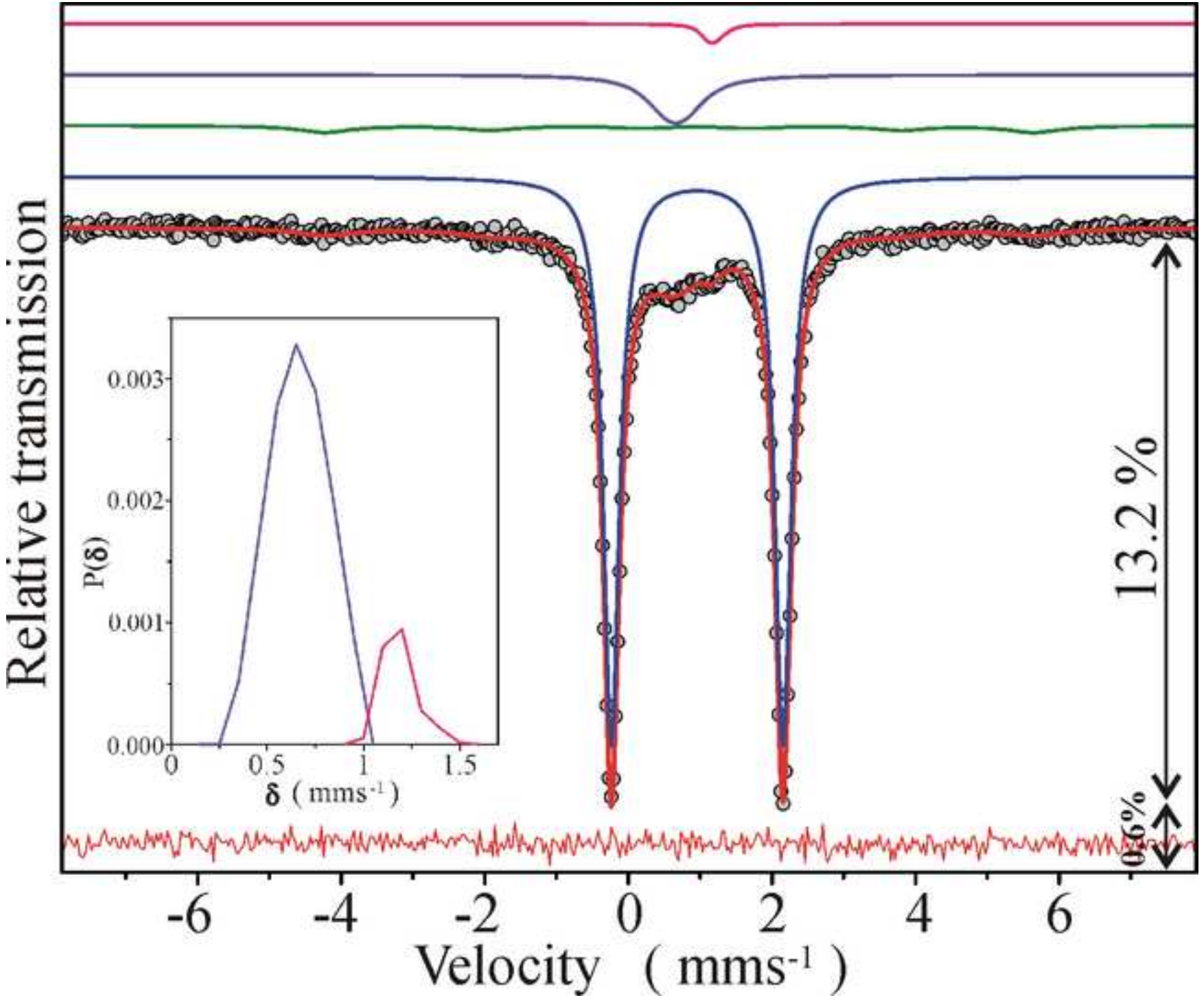
Relative transmission
13.2 %
0.6%
-6
-4
-2
0
2
4
6
Velocity (mms-1)
P(δ)
0.003
0.002
0.001
0.000
0
0.5
1
1.5
δ (mms-1)

Figure 6a

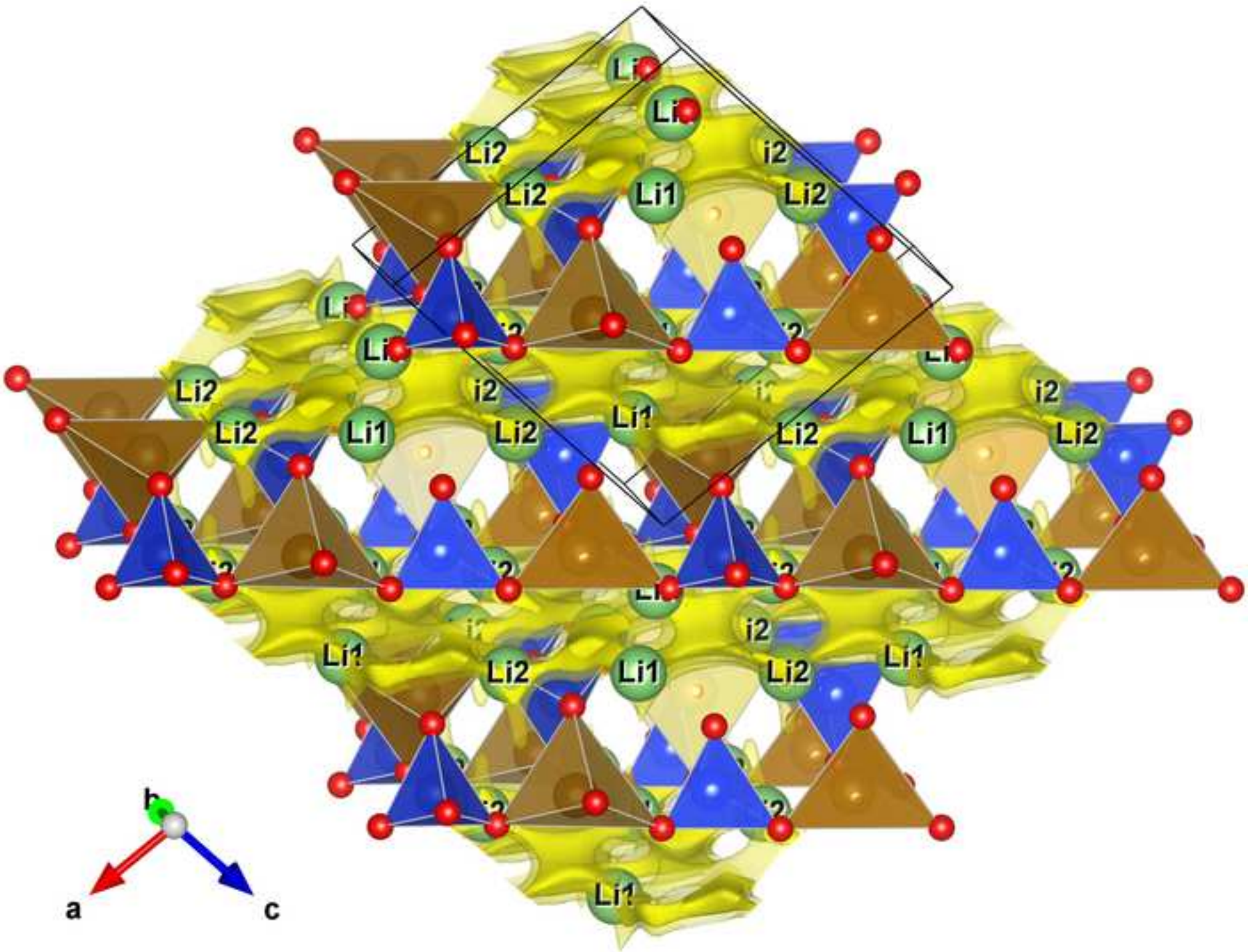
Li2
Li1
Li2
Li1
Li2
Li1
Li2
Li2
Li1
Li2
Li1
Li2
Li2
Li1
Li2
Li1
Li2
Li1
a
b
c

Figure 6b

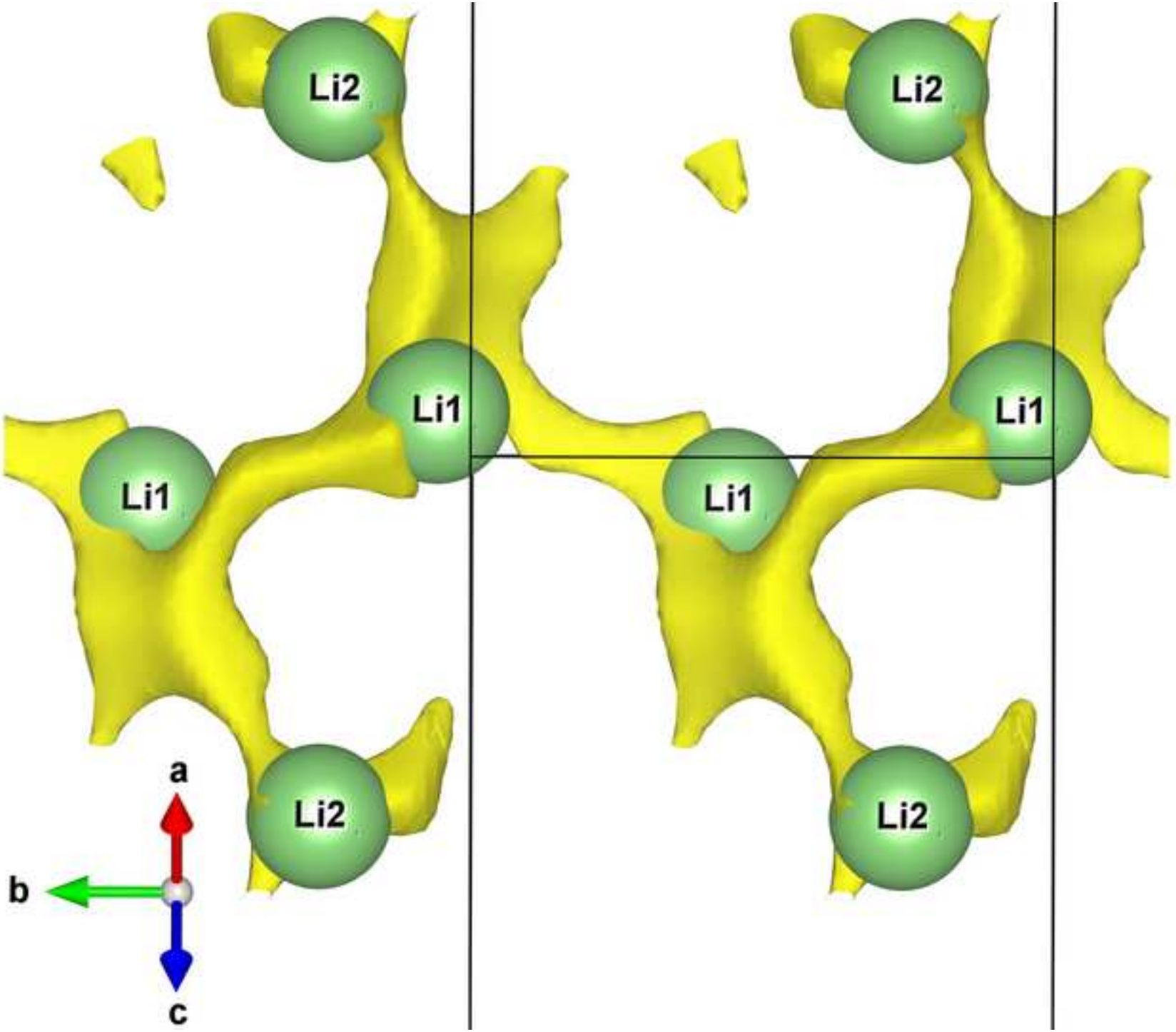

Figure 7

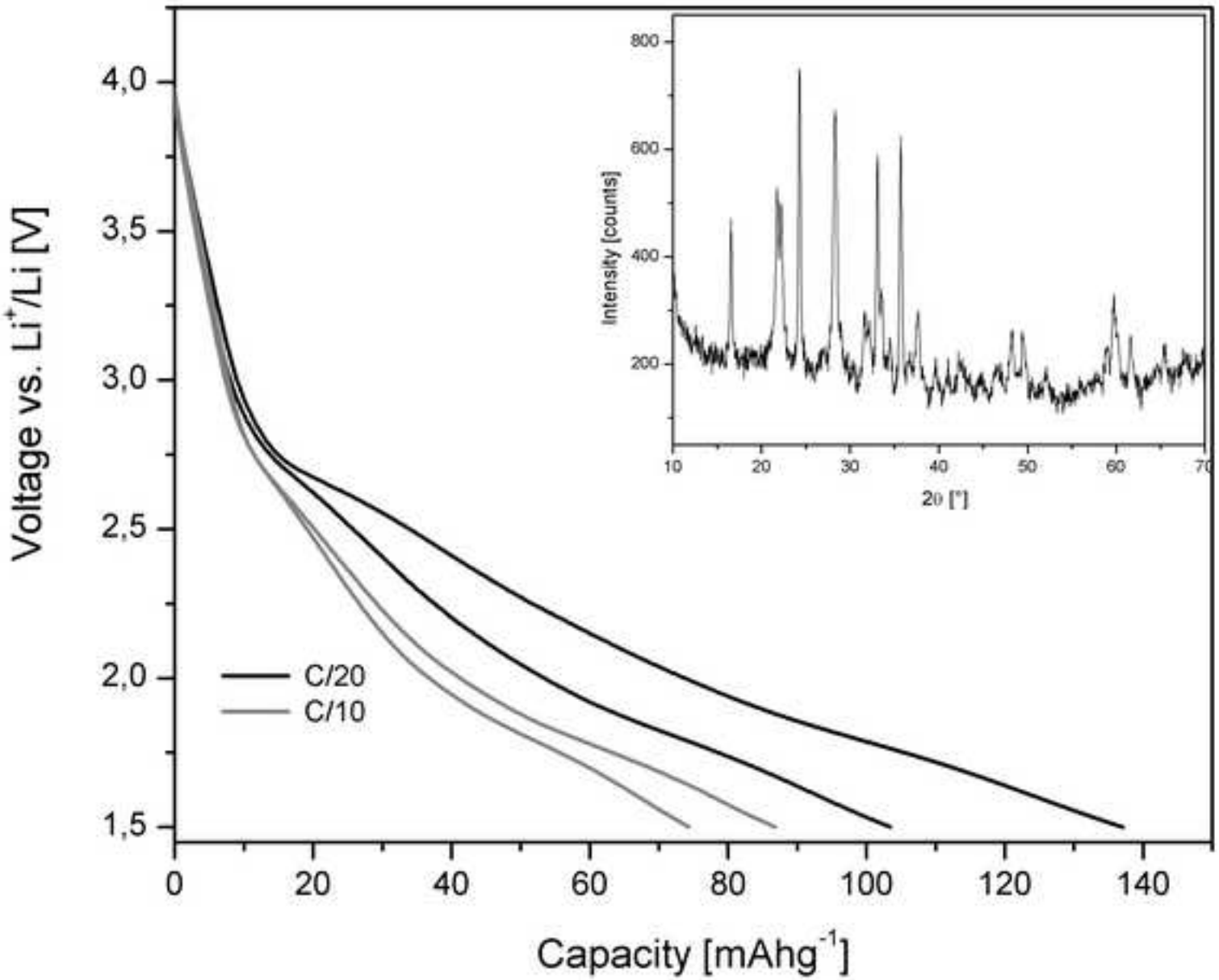
Voltage vs. Li+/Li [V]
4,0
3,5
3,0
2,5
2,0
1,5
0
20
40
60
80
100
120
140
Capacity [mAhg-1]
C/20
C/10
Intensity [counts]
800
600
400
200
10
20
30
40
50
60
70
2θ [°]